Low-temperature synthesis, structure and magnetoresistance of submicrometric $La_{1-x}K_xMnO_{3+\delta}$ perovskites

Yolanda Ng-Lee,[a†] Fernando Sapiña,[a†] Eduardo Martinez-Tamayo,[a†] José-Vicente Folgado,[a†] Rafael Ibañez,[a†] Daniel Beltrán,[a†] Francisco Lloret[b] and Alfredo Segura[a‡]

[a]*Institut de Ciència dels Materials de la Universitat de València, C/Doctor Moliner 50, 46100 Burjassot, Spain*
[b]*Departament de Química Inorganica, Universitat de València, C/Doctor Moliner 50, 46100 Burjassot, Spain*

The use of a precursor-based synthetic method, namely, the freeze-drying of acetic acid solutions, allows the preparation, at temperatures as low as 600 °C, of single phase perovskites in the solid solution series $La_{1-x}K_xMnO_{3+\delta}$. This soft treatment of the precursors yields products constituted of homogeneous nanometric particles (30–50 nm). Samples prepared at 1000 °C remain single phase for $x=0.00$, 0.05, 0.10 and 0.15, and are constituted by submicrometer homogeneous particles, without deviation from nominal stoichiometries upon heating. Their crystal structures were refined by the Rietveld method from X-ray powder diffraction data. Ac susceptibility, magnetization, resistivity and magnetoresistivity measurements have allowed us to establish, for the first time, relevant points of the electronic phase diagram of an alkali-metal-doped lanthanide manganate system.

The recent discovery of magnetoresistance in alkaline-earth-doped lanthanide manganates $Ln_{1-x}A_xMnO_{3+\delta}$ (Ln = La, Pr, Nd, Sm; A = Ca, Sr, Ba, Pb)[1] has attracted considerable interest in these materials which have, on the other hand, other properties that make them useful as catalysts or as state-of-the-art materials for cathodes in solid oxide fuel cells ($La_{0.86}Sr_{0.14}MnO_3$).[2] In fact, the magnetic and electric properties of these materials have been known for a long time,[3] however there is no satisfactory model accounting for the associated phenomenon that has been referred to as colossal magnetoresistance.[4,5] Notwithstanding, systematic explorations of mixed-valence lanthanide manganates have shown the relevance of both the mean oxidation state of manganese ions,[6] and the mean size of A cations in the resulting electronic properties of this type of material.[7]

While systematic investigations have been carried out on alkaline-earth-doped lanthanide manganites, references to magnetic and electronic properties of alkali-metal-doped materials are very scarce. Thus, although the preparation of potassium-doped compounds was reported twenty years ago,[8] the measurement of transport and magnetotransport properties on some aleatory compositions has only been accomplished very recently.[9] Nevertheless, under the reported synthetic conditions (ceramic method, thermal treatment at 1120 °C), losses of potassium and manganese are systematically observed. A similar effect has been observed in the preparation of other potassium mixed oxides, as in the case of potassium-doped $BaBiO_3$ superconducting materials,[10] which indicates the difficulties in controlling cation stoichiometry by this synthetic method.

At this point, to progress in the understanding of magnetic and transport properties of $La_{1-x}K_xMnO_{3+\delta}$ derivatives, it is necessary to accurately control the synthetic variables. The use of low-temperature methods can play an essential role in order to avoid potassium loss. In fact, freeze-drying has proved to be a powerful and versatile technique for mild preparation of complex oxides.[11] On the basis of the success of this synthetic approach, we have been able to establish relevant points in the electronic phase diagram (as a function of the composition) in the $La_{1-x}K_xMnO_{3+\delta}$ system.

Experimental

Aqueous solutions of metal acetates with molar nominal compositions La : K : Mn = $1-x$: x : 1.00 ($x=0.00$, 0.05, 0.10, 0.15, 0.20, 0.25) were prepared as follows. $KHCO_3$ was dissolved in 100 ml of glacial acetic acid. The addition of La_2O_3 led to a suspension, which was gently heated while stirring for 15 min. After addition of 20 ml of water, a transparent solution resulted. After cooling, $Mn(CH_3COO)_2{\cdot}4H_2O$ was added and dissolved upon stirring. The masses of the different reagents were adjusted to give 5 g of perovskite. Droplets of the resulting pale pink acetic acid solutions were flash frozen by projection on liquid nitrogen and then freeze-dried at a pressure of 10^{-2} atm. In this way, dried solid precursors were obtained as pink loose powders.

Preliminary measurements show that 600 °C is the minimum temperature at which the perovskite phase is obtainable (12 h) for all compositions investigated in this work, and was thus adopted for thermal treatment of the perovskite precursors. After cooling of the furnace, the samples were ground and heated under dynamic oxygen at 950 °C for 48 h. The resulting powders were then ground, pelletized and heated under a dynamic oxygen atmosphere at 1000 °C for 48 h.

Lanthanum, potassium and manganese contents were determined by atomic absorption using a Perkin-Elmer 300 AA spectrophotometer. The mean oxidation state of manganese ions and, therefore, the oxygen content, was determined by redox back-titration of Fe^{II} with potassium dichromate in HCl using a Crison CompacT Titrator.

Powder diffraction patterns were obtained using a Siemens D501 diffractometer, using secondary graphite-monochromated Cu-Kα radiation. In order to reduce preferred orientation, the samples were dusted through a sieve on the holder surface. All X-ray data analyses were performed using the FULLPROF program.[12]

Thermogravimetry (TG) was carried out using a Perkin-Elmer 7 system. The microstructure of the samples was observed with a Hitachi S-4100 field emission scanning electron microscope.

Ac susceptibility measurements were performed using a Lake Shore Cryotonics Inc. Model 7000 ac equipment in the temperature range 77–325 K. The frequency and exciting field amplitude used were 333.3 Hz and 1 Oe, respectively. Magnetization measurements were performed on a pendulum-type susceptometer in the temperature range 77–300 K at 1.23 T. Magnetization measurements at 77 K were performed working with magnetic fields up to 1.0 T.

Dc resistivity measurements were performed on sintered pellets with a standard four-probe technique. Measurements in the temperature range 30–300 K were performed in a He

† UIBCM.
‡ Grupo de Semiconductores.

closed-cycle Leybold–Heraeus cryostat while measurements in the range 300–350 K were performed in a laboratory implemented system operating under vacuum. In both cases, measurements were performed at zero field, and in a magnetic field of 0.6 T. The samples had approximately the same dimensions (typically $1.0 \times 3.0 \times 4.0$ mm).

Results and Discussion

Pyrolysis of the precursors

Thermal evolution of the precursors was monitored by means of TG and X-ray powder diffractometry.

The TG curves corresponding to the thermal evolution in oxygen atmosphere (heating rate 5 °C min^{-1}, flow rate 50 cm^3 min^{-1}) of the freeze-dried powder precursors show two sharp mass losses at 65 and 220 °C. No significant difference is observed between the different samples. The first step is associated with the evolution of acetic acid and/or water molecules retained in the precursor. The second mass loss fits well with the thermal decomposition of the metal acetate complex. Upon heating at higher temperatures, an additional very small mass loss is observed, associated to the decomposition of small quantities of carbonates and/or oxocarbonates formed during the decarboxylation process.

Fig. 1 shows X-ray powder diffraction patterns of the products that result from the thermal treatment of the $x = 0.05$ precursor at 600, 700, 800 and 900 °C in a tubular furnace during 12 h, under a dynamic oxygen atmosphere. This behaviour is representative of those obtained for all the compositions. Fig. 2 shows X-ray powder diffraction patterns of the products that result from treatment at 900 °C of the precursors for all the compositions explored in this work.

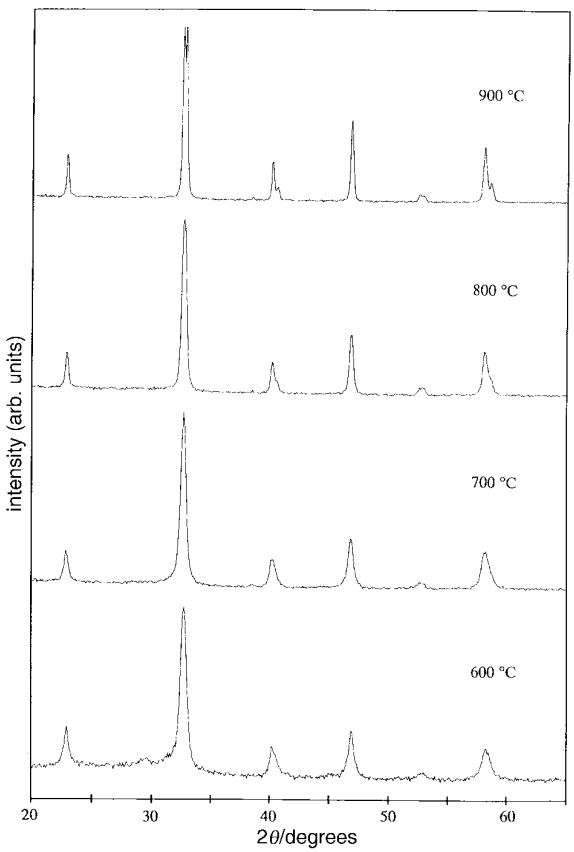

Fig. 1 X-Ray powder diffraction patterns of products resulting from the thermal treatment at 600, 700, 800 and 900 °C of the freeze-dried powder precursors with $x = 0.05$

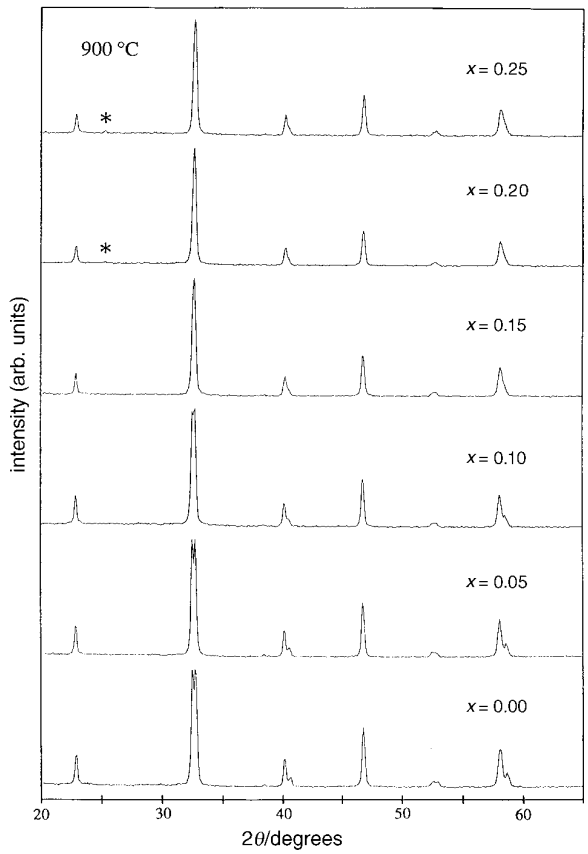

Fig. 2 X-Ray powder diffraction patterns of products resulting from the thermal treatment at 900 °C of the freeze-dried powder precursors with $x = 0.00$, 0.05, 0.10, 0.15, 0.20 and 0.25. Peaks marked * correspond to a K–Mn secondary phase.

The most remarkable feature of these patterns is the observation, at a temperature as low as 600 °C, of the perovskite as a nearly single phase for all the studied compositions. Extended thermal treatment at 600 °C confirm that single phase perovskites are obtained at this temperature. Patterns of samples treated at 500 °C show that perovskite is already the major phase, but the observation of intense reflections associated with intermediate phases indicates that the reaction is not complete.

Scanning electron microscopy (field emission) images show that samples prepared at 600 °C are constituted of homogeneous particles, ranging in size from 30 to 50 nm. A progressive increase in the particle size is observed in samples prepared at higher temperatures. Thus, at 900 °C, samples are constituted by homogeneous well faceted particles of sizes between 80 and 140 nm. For samples pelletized and sintered at 1000 °C for 48 h, particles have grown appreciably (130–500 nm).

Chemical characterization

Table 1 summarizes the results of the chemical analysis of samples sintered at 1000 °C. As can be observed, the actual potassium content for the $x = 0.05$, 0.10 and 0.15 samples is practically equal to the nominal one. However, in samples of nominal composition $x = 0.20$ and 0.25, small departures from the initial compositions are detected, indicating loss of potassium during the preparation and sinterization processes. For these compositions X-ray diffraction shows (even for samples prepared at 900 °C) the presence of the secondary phase $K_2Mn_4O_8$[13] although no segregation is observed by SEM. These results suggest the existence of a potassium solubility limit in this system, as might be inferred from results of

Table 1 Chemical analysis for samples of nominal composition $La_{1-x}K_xMnO_{3+\delta}$

x	La/Mn	K/Mn	% Mn^{4+}	δ	stoichiometry
0.00	1.00	0.00	34	0.17	$La_{0.946}Mn_{0.946}O_3$
0.05	0.96	0.04	33	0.12	$La_{0.924}K_{0.039}Mn_{0.963}O_3$
0.10	0.90	0.11	31	0.06	$La_{0.882}K_{0.108}Mn_{0.981}O_3$
0.15	0.84	0.15	32	0.01	$La_{0.837}K_{0.150}Mn_{0.997}O_3$
0.20	0.80	0.18	42	—	
0.25	0.76	0.22	52	—	

previous work.[8] Thus, the following discussion refers to the $x=0.00$, 0.05, 0.10 and 0.15 samples.

The oxygen content of these four samples has been determined from the analytically calculated value of the mean oxidation state of the manganese ions and metal content (Table 1). As can be observed, the mean manganese oxidation state is practically constant, at 3.33 ± 0.02 for the four samples. Indeed, the effect of the increase in the potassium content is a decrease of the oxygen excess (for $x=0.00$, $\delta=0.17$; for $x=0.15$, $\delta=0.01$).

The above results show that, in contrast to the ceramic procedure,[9] the formation of the perovskite phase incorporating the potassium into the lattice at low temperature allows reliable stoichiometry control.

Structural characterization

The structures of the perovskite phases have been refined in the space group $R\bar{3}c$, in the hexagonal setting, from room-temperature powder X-ray diffraction data of samples prepared at 1000 °C. The starting structural model used was that of $La_{0.95}Mn_{0.95}O_3$.[14] The fits were performed using a pseudo-Voigt peak-shape function. In the final runs, usual profile parameters (scale factors, background coefficients, zero points, half-width, pseudo-Voigt and asymmetry parameters for the peak shape), atomic positions and thermal parameters were refined. In the structural models, La and K are considered to be disordered in A sites, and their occupancies were fixed to give the oxygen stoichiometry and metal contents obtained by chemical analysis. The results of the refinements are given in Table 2 while Table 3 lists selected bond distances and angles, as well as cell parameters for rhombohedral setting.

Table 2 Structural data from X-ray powder diffraction studies of $La_{1-x}K_xMnO_{3+\delta}$[a]

	$x=0.00$	$x=0.05$	$x=0.10$	$x=0.15$
a/Å	5.5179(6)	5.5148(7)	5.5123(7)	5.5061(9)
c/Å	13.3463(7)	13.3588(7)	13.3742(7)	13.3843(10)
$B_{La,K}$/Å^2	1.80(4)	1.58(4)	1.90(4)	1.80(4)
n_{La}	0.946	0.924	0.882	0.837
n_K	0.000	0.039	0.108	0.150
B_{Mn}/Å^2	1.13(5)	0.96(5)	1.37(5)	1.83(5)
n_{Mn}	0.946	0.963	0.981	0.997
x_O	−0.5501(11)	−0.5462(12)	−0.5455(13)	−0.5432(14)
B_O/Å^2	1.85(15)	1.58(14)	1.97(15)	2.26(15)
n_O	1.000	1.000	1.000	1.000
R_p	5.24	5.64	4.76	5.09
R_{wp}	7.03	7.62	6.32	6.98
χ^2	2.59	2.70	2.56	2.58
R_B	1.96	2.14	2.45	2.81
R_F	2.78	3.18	4.16	3.75

[a]Space group $R\bar{3}c$, Hexagonal setting. La, K (6a): (0, 0, 1/4); Mn (6b): (0, 0, 0); O (18e): (x, 0, 1/4).

With respect to ideal cubic structure, characterized by regular 12-coordination for A cations, and a B—O—B angle of 180°, the rhombohedral structure presents irregular 12-coordination around cation A, and a B—O—B angle that deviates substantially from 180°. This structural distortion can be thought of as being produced by rotations of the BO_6 octahedra ($a^-a^-a^-$ tilt system in Glazer's notation).[15] As can be observed in Table 3, the rhombohedral distortion progressively decreases with the substitution of La^{3+} by the larger K^+ cation. For $x=0.00$ the spread of A—O distances and O—Mn—O angles are 0.55 Å and 2°, and decrease to 0.47 Å and 1.4° for $x=0.15$. In the same way, the Mn—O—Mn angle increases from 163.8(3) ($x=0.00$) to 166.2(3)° ($x=0.15$), and the rhombohedral angle α_r decreases from 60.56 ($x=0.00$) to 60.34° ($x=0.15$).

Magnetic properties

We have measured the isothermal magnetization $M(T, H)$ at 77 K with fields up to 10 000 Oe, after cooling in zero magnetic field. For fields higher than 3000 Oe, the magnetic moment is saturated, and $M(77\text{ K}, H)$ changes linearly with the field. A linear extrapolation at $H=0$ allows us to derive the spontaneous magnetization, M_S (77 K) and, thus, the net magnetic moment per Mn ion in the direction of the magnetization, μ_B (77 K). The results are presented in Table 4. The net magnetic moment per Mn ion shows clearly that the samples present a ferromagnetic moment at 77 K. Except for $x=0.00$, the observed magnetic moments are in all cases very close to the theoretic single-ion values, taking into account the mixed valence of Mn ions in these compounds. This indicates that the $x=0.00$ sample presents a non-collinear ferromagnetic structure.

The temperature dependence of the magnetization was measured in a field of 12 300 Oe in heating runs, for temperatures ranging from 77 to 300 K. The curves in Fig. 3(*a*) and (*c*) are for $x=0.00$ and $x=0.05$, respectively; the latter also being representative of the behaviour of the $x=0.10$ and 0.15 samples. The magnetization decreases as the temperature increases, and drops corresponding to a ferromagnetic to paramagnetic phase transition. Estimated transition temperatures, T_M, are given in Table 4. The sample $x=0.15$ is ferromagnetic even at the highest temperatures used.

The ferromagnetic phase transition temperatures for $x=0.00$, 0.05 and 0.10 were verified by measuring the thermal dependence of both the in-phase, χ', and the out-of-phase, χ'', components of the ac magnetic susceptibility, for temperatures in the range 77–325 K. Fig. 3(*b*) and (*d*) show the thermal variation of the in-phase component of the ac susceptibility for $x=0.00$ and 0.05. The χ' curves show an abrupt break at

Table 3 Selected bond distances (Å) and angles (degrees) and cell parameters for the rhombohedral cells of $La_{1-x}K_xMnO_{3+\delta}$

	$x=0.00$	$x=0.05$	$x=0.10$	$x=0.15$
Mn—O	1.962(3) (×6)	1.959(3) (×6)	1.959(3) (×6)	1.956(4) (×6)
O—Mn—O	91.0(2) (×6)	90.9(3) (×6)	90.8(3) (×6)	90.7(3) (×6)
	89.0(2) (×6)	89.1(2) (×6)	89.2(3) (×6)	89.3(3) (×6)
Mn—O—Mn	163.8(3)	165.0(3)	165.3(3)	166.2(3)
La—O	2.750(3) (×6)	2.749(3) (×6)	2.750(3) (×6)	2.749(3) (×6)
	2.482(3) (×3)	2.502(4) (×3)	2.505(5) (×3)	2.519(5) (×3)
	3.036(4) (×3)	3.012(4) (×3)	3.007(4) (×3)	2.988(5) (×3)
a_r/Å	5.4717	5.4743	5.4776	5.4780
α_r/°	60.56	60.49	60.42	60.34

Table 4 Spontaneous magnetization and characteristic temperatures obtained from magnetization, ac magnetic susceptibility, transport and magnetotransport measurements

	$x=0.00$	$x=0.05$	$x=0.10$	$x=0.15$
μ_B (77 K)	2.30	3.25	3.29	3.24
μ_B (calc.)	3.66	3.67	3.69	3.68
T_M	150	235	305[a]	325[a]
T_c	150	235	305	—
T_r	165[b]	185	270	280
T_{MR}	170[b]	225	295	320

[a]Temperature estimated from data taken up to 300 K. [b]Temperatures of change between the insulator regime and the appearance of magnetoresistance.

T_c as the temperature is lowered, which coincides with the appearance of an out-of-phase signal in the χ'' curves. This behaviour clearly indicates that the system undergoes a phase transition from a paramagnetic to a long-range ordered magnetic state with a ferromagnetic component. T_c values are listed in Table 4. Upon further cooling, both χ' and χ'' reach a maximum, and then decrease, owing to the formation of magnetic domains in the ferromagnetic ordered samples.

Transport and magnetotransport properties

Fig. 3(*a*) and (*c*) show the temperature dependence of the resistivity at zero field for the $x=0.00$ and 0.05 samples, the latter behaving similarly to the $x=0.10$ and 0.15 samples. Except for $x=0.00$, all samples exhibit a change in electrical properties upon cooling, from insulator to metallic-like behaviour. Thus, a maximum in the resistivity *vs.* temperature curves, characteristic of a semiconductor-to-metal transition, is observed at a temperature T_r, close to the temperature at which spontaneous magnetization appears and T_r values are given in Table 4. The sample $x=0.00$ behaves as a semiconductor over the entire temperature range investigated, but presents two different regimes.

Application of a magnetic field reduces significantly the resistivity below the transition temperature. Fig. 3(*b*) and (*d*) show thermal variation of the magnetoresistance, defined as $-[\rho(T,H)-\rho(T,0)]/\rho(T,0)$, for $x=0.00$ and 0.05. Upon cooling, a peak in the magnetoresistance is observed at temperatures T_{MR} (see Table 4), very close to the paramagnetic insulator–ferromagnetic metal transition, for $x=0.05$, 0.10 and 0.15. At low temperatures, the magnetoresistance increases continuously. However, for the sample $x=0.00$, magnetoresistance begins to increase upon further cooling at temperatures close to T_c.

The above observations can be summarized by construction of an electronic phase diagram for the system $La_{1-x}K_xMnO_{3+\delta}$ (Fig. 4). Several electronic phases are observed. At low temperature, samples are ferromagnetic metals for $x\geqslant 0.05$ (FM). The sample $x=0.00$ is a non-collinear ferromagnetic insulator (NCFI). At high temperatures, all the samples behave as paramagnetic insulators (PMI). The transition temperature increases with x, reaching a maximum value at $x=$ 0.15 (325 K).

Although this phase diagram is similar to those previously reported for alkaline-earth-doped systems,[6] one significant difference should be pointed out. Until now, two different parameters have been considered to be relevant concerning the electronic behaviour of these compounds, namely, the concentration of Mn^{4+}, c (directly related with the concentration of carriers in e_g orbitals) and the mean size of cations in A positions, $\langle r_A\rangle$. The reported electronic phase diagram of $La_{1-x}Sr_xMnO_3$ ($0\leqslant x\leqslant 0.6$) corresponds to samples with a variable concentration of carriers. While the concentration of carriers in $La_{1-x}Ca_xMnO_3$ ($0\leqslant x\leqslant 1$) has not been measured, from the analysis of published results, it is evident that c varies in the whole or in a large part of the phase diagram. The phase diagram of the $La_{1-x}K_xMnO_{3+\delta}$ system reported in this work corresponds to samples with a constant concentration of Mn^{4+}. Consequently, these three phase diagrams correspond to different two-dimensional representations of the three-dimensional (T, c, $\langle r_A\rangle$) phase diagram.

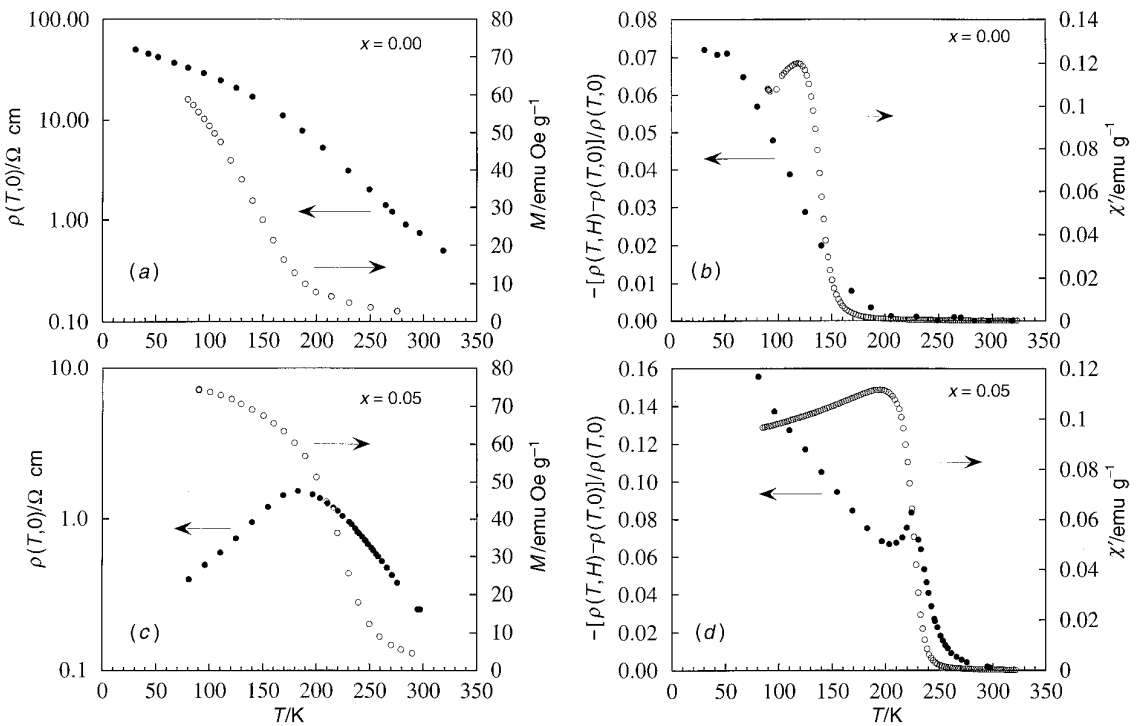

Fig. 3 (*a*), (*c*) Thermal variation of magnetization and zero-field resistivity for $x=0.00$ and 0.05 samples. (*b*), (*d*) In-phase component of the ac susceptibility and magnetoresistance (applied field 0.6 T) for $x=0.00$ and 0.05 samples.

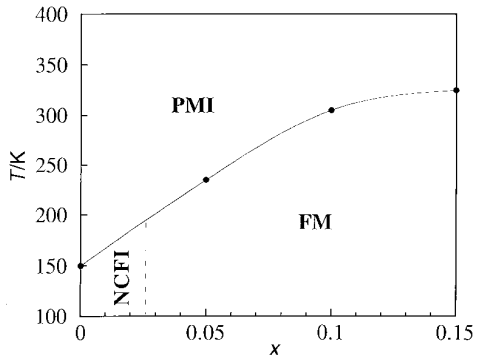

Fig. 4 Electronic phase diagram of $La_{1-x}K_xMnO_{3+\delta}$

On the other hand, our results suggest that c and $\langle r_A \rangle$ are not the only parameters which need to be considered in the description of the electronic phase diagrams of these systems. Consider the sample with $x=0.00$, for which c is 34%. This sample can then be compared with the reported behaviour[7] of a sample with composition $La_{0.7}Ca_{0.3}MnO_3$. Since La^{3+} is larger than Ca^{2+}, it must be expected that our sample with $x=0.00$ would show a transition from paramagnetic-insulating to ferromagnetic-metallic behaviour at temperatures above 240 K. However, the sample $x=0.00$ actually shows a transition from paramagnetic-insulating to ferromagnetic-insulating at 160 K. Thus, it must be concluded that the parameters c and $\langle r_A \rangle$ alone do not characterize the behaviour of this sample.

The seemingly anomalous behaviour of the sample with $x=0.00$, as well as the reported behaviour of samples with different La : Mn ratios can be understood considering the concentration of vacancies in B positions, v_B, as an additional parameter. Studies of polycrystalline samples[16–18] and thin films[19] with different La : Mn ratios have shown that low temperatures of magnetic ordering and semiconducting behaviour are associated with La : Mn ratios very close to 1.00 and, owing to the oxygen non-stoichiometry, to high values of v_B. On the other hand, a decrease in the La : Mn ratio and, thus, in v_B, leads to a semiconductor–metal transition, and to an increase in the ordering temperature which results, in these cases, to behaviour very close to that expected from the above mentioned considerations. Although this effect must be probably associated with the scattering of carriers by the vacancies, careful experiments must be designed in order to determine if structural modifications induced by vacancies are also involved in electronic phase transitions.

In conclusion, the use of a precursor-based synthetic method, namely, freeze drying of acetic acid solutions, enables the formation of single-phase perovskites at low temperatures. The formation of the perovskite phase incorporating potassium into the lattice at low temperatures avoids their evaporation at high temperatures and allows, in contrast with the ceramic procedure, a reliable control of stoichiometry. Our preliminary results indicate that the same strategy is also valid for sodium-doped materials.[20] The availability of samples with controlled stoichiometry has allowed the measurement, for the first time, of relevant points in the electronic phase diagram of an alkali-metal-doped lanthanide manganate system.

This research was supported by the Spanish Comision Interministerial de Ciencia y Tecnología (CICYT, MAT93-0240-CO4-O2, MAT96-1037-CO2-O1) and the Generalitat Valenciana (GV-1126/93, GV-2227/94). The SCSIE of the Universitat de València is acknowledged for X-ray diffraction, SEM and analytical facilities. Y. Ng acknowledges the financial support of CDCH of the UCV for her stay in Spain.

References

1 (*a*) R. M. Kusters, J. Singleton, D. A. Keen, R. McGreevy and W. Hayes, *Phys. B*, 1989, **155**, 362; (*b*) R. von Helmot, J. Wecker, B. Holzapfel, L. Schultz and K. Samwer, *Phys. Rev. Lett*., 1993, **71**, 2331; (*c*) S. Jin, T. H. Tiefel, M. McCormack, R. A. Fastnacht, R. L. Ramesh and H. Chen, *Science*, 1994, **64**, 413.
2 (*a*) L. G. Tejuca, J. L. Fierro and J. M. D. Tascón, *Adv. Catal*., 1989, **36**, 237 and references therein; (*b*) N. Q. Minh, *J. Am. Ceram. Soc*., 1993, **76**, 563 and references therein.
3 E. O. Wollan and W. C. Koeller, *Phys. Rev. B*, 1955, **100**, 545.
4 (*a*) A. Maignan, Ch. Simon, V. Caignert and B. Raveau, *Solid State Commun*., 1995, **96**, 623; (*b*) R. Mahendiran, S. K. Tiwary, A. K. Raychaudhuri, R. Mahesh, N. Rangavittal and C. N. R. Rao, *Phys. Rev. B*, 1996, **53**, 3348; (*c*) H. L. Ju, J. Gopalakrishnan, J. L. Peng, Qi Li, G. C. Xiong, T. Venkatesan and R. L. Greene, *Phys. Rev. B*, 1995, **51**, 6143.
5 (*a*) A. J. Millis, P. B. Littlewood and B. I. Shraiman, *Phys. Rev. Lett*., 1995, **74**, 5144; (*b*) H. Röder, J. Zang and A. R. Bishop, *Phys. Rev. Lett*., 1996, **76**, 1356.
6 (*a*) P. Schiffer, A. P. Ramirez, W. Bao and S. W. Vheong, *Phys. Rev. Lett*., 1995, **75**, 3336; (*b*) A. Urushibara, Y. Moritomo, T. Arima, A. Asamitsu, G. Kido and Y. Tokura, *Phys. Rev. B*, 1995, **51**, 14103.
7 (*a*) A. Maignan, V. Caignert, Ch. Simon, M. Hervieu and B. Raveau, *J. Mater. Chem*., 1995, **5**, 1091; (*b*) H. Y. Hwang, S. W. Cheong, P. G. Radaelli, M. Marezio and B. Batlogg, *Phys. Rev. Lett*., 1995, **75**, 914; (*c*) R. Mahesh, R. Mahendiran, A. K. Raychaudhuri and C. N. R. Rao, *J. Solid State Chem*., 1995, **120**, 204.
8 R. J. H. Voorhoeve, J. P. Remeika, L. E. Trimble, A. S. Cooper, F. J. Disalvo and P. K. Gallagher, *J. Solid State Chem*., 1975, **14**, 395.
9 T. Shimura, T. Hayashi, Y. Inaguma and M. Itoh, *J. Solid State Chem*., 1996, **124**, 250.
10 G. V. Rama Rao, U. V. Varadaraju and S. L. Mannan, *Physica C*, 1994, **235–240**, 761.
11 D. Beltrán, A. Beltrán, R. Ibañez, F. Sapiña, M. J. Sanchis, V. Primo, H. Miao, J. García, R. Carrasco, P. Amorós, J. V. Folgado, E. Escrivá and E. Martinez, *Superconductivity in Spain* (*1990–1992 Research Activities*), ed. F. Yndurain, Madrid, Spain, 1993, p. 37.
12 J. Rodriguez-Carvajal, FULLPROF Program, personal communication.
13 PDF-2 Database, JCPDS-ICDD No. 160205.
14 J. A. M. van Roosmalen, E. H. P. Cordfunke, R. B. Helmholdt and H. W. Zandbergen, *J. Solid State Chem*., 1994, **110**, 100.
15 A. M. Glazer, *Acta Crystallogr., Sect. B*, 1972, **28**, 3384.
16 V. Ferris, L. Brohan, M. Ganne and M. Tournoux, *Eur. J. Solid State Inorg. Chem*., 1995, **32**, 131.
17 A. Arulraj, R. Mahesh, G. N. Subbanna, R. Mahendiran, A. K. Raychaudhuri and C. N. R. Rao, *J. Solid State Chem*., 1996, **127**, 87.
18 J. Töpfer, J. P. Doumerc and J. C. Grenier, *J. Mater. Res*., 1996, **6**, 1511.
19 A. Gupta, T. R. McGuire, P. R. Duncombe, M. Rupp, J. Z. Sun, W. J. Gallagher and G. Xiao, *Appl. Phys. Lett*., 1995, **67**, 3494.
20 F. Sapiña, P. Majewski, E. Martinez-Tamayo, R. Ibañez, D. Beltrán and F. Lloret, manuscript in preparation.

Paper 6/07090F; *Received* 17*th October*, 1996